Characterization of a new open cylindrical ion cyclotron resonance cell with unusual geometry

B. Kanawati[a] and K. P. Wanczek[b]
Department of Physical and Inorganic Chemistry, University of Bremen, Bremen, Germany

(Received 29 January 2007; accepted 29 May 2007; published online 3 July 2007)

A new cylindrical ion cyclotron resonance cell with electrodes of different diameters is characterized. It consists of a central segmented electrode for ion trapping and detection and two planar trapping electrodes with a center bore, to which two small tube electrodes are fitted. The cell can trap either positive or negative ions or both ion polarities in the center region. For trapping both ion polarities, an unsymmetrical double well potential can be generated. Ions generated from SF_6 by electron impact or electron attachment are investigated. In depth analysis of radial excitation patterns of positive and negative ions trapped simultaneously in different stability regions reveals sharp discrimination in the extent of radial acceleration. SIMION simulations of the radial excitation show different trajectories of positive and negative ions. Axial component of radial dipolar excitation field exists in the terminal stability regions. © *2007 American Institute of Physics.*
[DOI: 10.1063/1.2751100]

I. INTRODUCTION

Ion cyclotron resonance[1] (ICR) cells with different geometries were designed and tested by several authors.[2–4] A review of these designs is available in the literature.[5] Each ICR cell geometry has characteristic features and problems to be overcome in order to achieve important objectives such as high resolution, high dynamic range and signal/noise ratio, and high trapping effectivity at high pressures, in addition to the capability of trapping and detecting positive and negative ions simultaneously.

Although Penning traps[6,7] with hyperbolical electrodes are able to produce the most ideal quadrupolar axial and radial potential forms, they are limited to the study of one ion polarity. Expanding this limit to trap both positive and negative ions requires more complex cell geometries such as five section cylindrical ICR cells. Open multisection cylindrical ICR cells are favored over closed ones, since they have a minimal axial component of ion acceleration during dipolar radial excitation event. In addition, they are capable of reaching lower pressures, since open geometries do not hinder pumping and facilitate faster particle removal out of the cell. Open cell geometries are also compatible with external ion sources such as electrospray ionization and laser ion sources. On the other hand, the quadrupolar approximation of these geometries is only valid in a very narrow region in the center of the ICR cell. Beyond this region, there is an axial anharmonicity of ion motion, which causes cyclotron frequency to depend on the axial trapping amplitude of ions. Although correction rings were designed and implemented[8] to prevent this dependence, there is a constant trend to design and probe new ICR cells for new purposes. At the same applied voltage, the potential values on open cylindrical ICR cells are lower and mass resolution is lower, in general, than in a classical closed cylindrical ICR cell.

Gabrielse *et al.*[9] have studied the possibility of simultaneous trapping of antiprotons and positrons and their recombination reactions in a nested ion trap. They emphasized the role of three body collisions in increasing the calculated rate for antihydrogen production starting from one antiproton and two positrons. Electron capture dissociation (ECD), which implies recombination of positive ions with low energy electrons in the gas phase, discovered by Zubarev *et al.*,[10] is another interesting subject which could be achieved experimentally in the ICR cell. However, ion-ion electron transfer dissociation (ETD) in the gas phase has been studied in rf Paul traps only until now.[11,12]

This article describes a new cell geometry which shares some benefits of both closed and open cylindrical geometries. The effective trapping potentials are higher than those achieved in normal open cylindrical cells at the same applied voltage, although it has an open geometry. This open geometry makes this cell compatible with external ion sources. Several electrodes are available to establish double well potential configuration to trap and detect both ion polarities simultaneously. Simultaneous trapping of both ion polarities could be achieved by several cell geometries[13–15] in the past.

The double well potential configuration of the new ICR cell was characterized experimentally and theoretically by SIMION[16] calculations. Discrimination in ion detection depending on the ion polarity was also observed in this new cell geometry and examined in detail.

It is interesting to see what kind of double well potential configurations can be implemented in this new ICR cell and what kind of radial potential patterns are available at different stability regions along the z axis.

[a]Author to whom correspondence should be addressed; electronic mail: kanawati@t-online.de
[b]Electronic mail: icrwan@icr.uni-bremen.de

II. EXPERIMENT

The experiments were done with the prototype Fourier transform (FT) ICR spectrometer CMS 47 (Bruker Daltonik, Bremen), equipped with a 7 T superconducting magnet. A simple UHV manifold was pumped with a turbomolecular pump (Pfeiffer, Wetzlar, TPU 240). The base pressure was below 10^{-9} mbar. Two inlet systems at a base pressure of 2×10^{-2} mbar were connected to the UHV system by Varian leak valves. For the experiments several digital-to-analog converter (DAC) cards, controlled by personal computers (PCs), were added and triggered by the main computer Aspect 3000 of the spectrometer. In this way the pulse sequences necessary for the experiments were generated. dc voltages between +9 and −9 V were applied. rf pulses were generated by an arbitrary wave form generator.

The experiments described in Sec. III were done with sulfur hexafluoride. Positive ions were generated by electron impact at 70 eV electron energy, and negative ions by attachment of thermalized electrons. Electrons were gated using a triggered gate located between the filament and the ICR cell. The gate potential was set up to be −60 V during the ionization pulse while the gate potential was −109 V in the closed mode. The duration of the ionizing electron beam was 20 ms for trapping effectivity experiments (2×10^{-6} mbar) and 200 ms for radial excitation experiments (2×10^{-7} mbar). The distance between the electron gate and the terminal tube of the ICR cell is 70 mm. This was sufficient to eliminate any interference of external electric fields generated from the gate itself on the potential configuration set up inside the ICR cell. Thus no gate influence exists on ion trajectories inside the ICR cell.

Trapping efficiency test was done under 2×10^{-6} mbar in the potential configurations 1/6/0/6/1 and −3/3/0/3/−3 for 15 s, whereby both ion polarities (SF_3^+ and SF_6^-) were trapped simultaneously in each potential configuration. In 1/6/0/6/1 both side electrodes were kept at +6 V and both terminal tube electrodes were kept at +1 V during the whole experiment. In −3/3/0/3/−3 both side electrodes were kept at +3 V and both terminal tube electrodes were kept at −3 V during the whole acquisition. All segments of the central ring electrode were grounded.

An automation program was written for the Aspect computer to control the experimental events inside the ICR cell. For experiments, that show signal intensity dependence on radial excitation level parameter XA in decibel, no ions were ejected after the end of ionization pulse. Thus, SF_5^+ signal as base peak was produced and is shown in Fig. 10.

III. RESULTS AND DISCUSSION

A. Description of the new ICR cell

Figure 1 shows the *yz*-midplane view of the new cell geometry. R1 and R2 are two stainless steel tube electrodes with an inner diameter of 10 mm and 2 mm wall thickness. Each tube electrode is 20 mm long. S1 and S2 are side electrodes, made from 2.5 mm thick material, which have a circular geometry with a hole of 14 mm inner diameter in the center of each in order to be compatible with the tube electrodes R1 and R2 mentioned above for installation. The outer diameter of the side electrode is 44 mm.

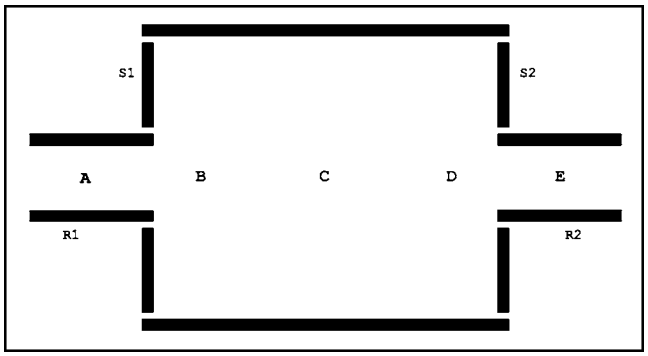

FIG. 1. Two-dimensional (2D) (*yz*) view for the new ICR cell. Ion detection is possible inside the region BCD.

The inner length of the ring electrode between S1 and S2 is 60 mm, and the inner diameter is 46 mm. The ring electrode consists of eight stainless steel segments. Each segment electrode of the eight segments is 1 mm thick. The distance between two neighboring segments in the eight segmented central electrode is 0.5 mm. Although quadrupolar radial ion excitation can be achieved by use of four segmented central electrode,[17] the central electrode in our ICR cell was originally segmented into eight segments to make the cell flexible in running quadrupolar radial excitation, without the need to switch two segments between excitation and detection circuits. In experiments described in this article, each two neighboring segments are wired together to allow for dipolar excitation and detection. In this way, ion detection sensitivity and excitation electric field strength are increased. The whole ICR cell assembly is surrounded with a grounded stainless steel tube, the UHV vacuum housing with an inner diameter of 82 mm.

The convention 1/6/0/6/1, for example, means that tube electrodes R1 and R2 are at +1 V each and the side electrodes S1 and S2 have +6 V each relative to the grounded central ring electrode. In this way, trapping of positive ions in the terminal regions A and E is not possible. This is desirable, since ions trapped there cannot be detected. Fur-

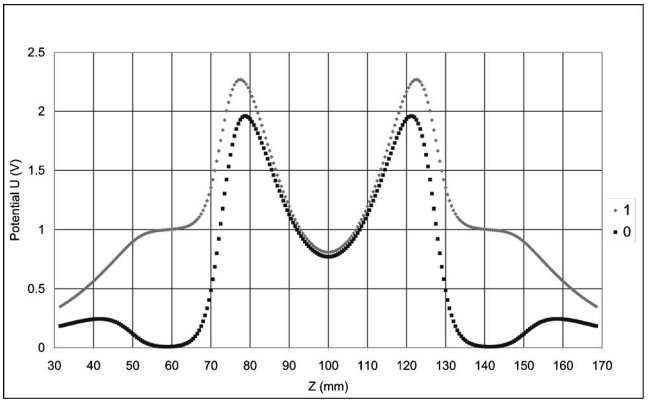

FIG. 2. Axial potential curve in the potential configuration 1/6/0/6/1 (♦) and 0/6/0/6/0 (■). The potential of each of tube electrodes R1 and R2 is shown in the legend at the right side of the diagram. Axial segments are as follows: R1, 50–70 mm; detection region between side electrodes S1 and S2, 70–130 mm; and R2, 130–150 mm.

thermore positive ions in regions A and E cannot be accelerated toward the center of the ICR cell by pulsing different voltages on both tube electrodes R1 and R2 relative to the grounded ring electrode in the range of −9−+9 V.

Using the above mentioned double hill potential configuration, positive ions can be trapped only in the central region C, while negative ions are trapped on both potential hills in regions B and D. This potential configuration has proven to be suitable for efficient trapping and detection of both polarities simultaneously, although the negative ions are discriminated (described in detail in Sec. III C 1).

B. SIMION calculations

1. Axial potential distribution and axial ion trajectories

Figure 2 shows the axial potential course along the z axis for the potential configurations 0/6/0/6/0 and 1/6/0/6/1. The potential configuration 0/6/0/6/0 can provide five stability regions (A–E; see Figs. 1 and 2) for trapping ions inside the cell.

However, ions trapped inside the terminal tube electrodes (stability regions A and E) cannot be radially excited for detection or axially excited toward the cell center for successive radial detection. To avoid trapping ions in the stability regions A and E, the potential configuration 1/6/0/6/1 was used instead. Note the monotonically falling electric potential curves in case of 1/6/0/6/1 in regions A (50–70 nm) and E (130–150 mm), which exclude all positive ions generated beyond the range of 70–130 mm.

Positive ions are trapped in the central deep potential minimum (90–110 mm), where Coulumbic cation-cation repulsion should be high, since ions are confined to a narrow potential minimum. This is the case for thermal positive ions.

Negative ions are trapped in two narrow and asymmetric potential maxima close to the outer regions of the large cen-

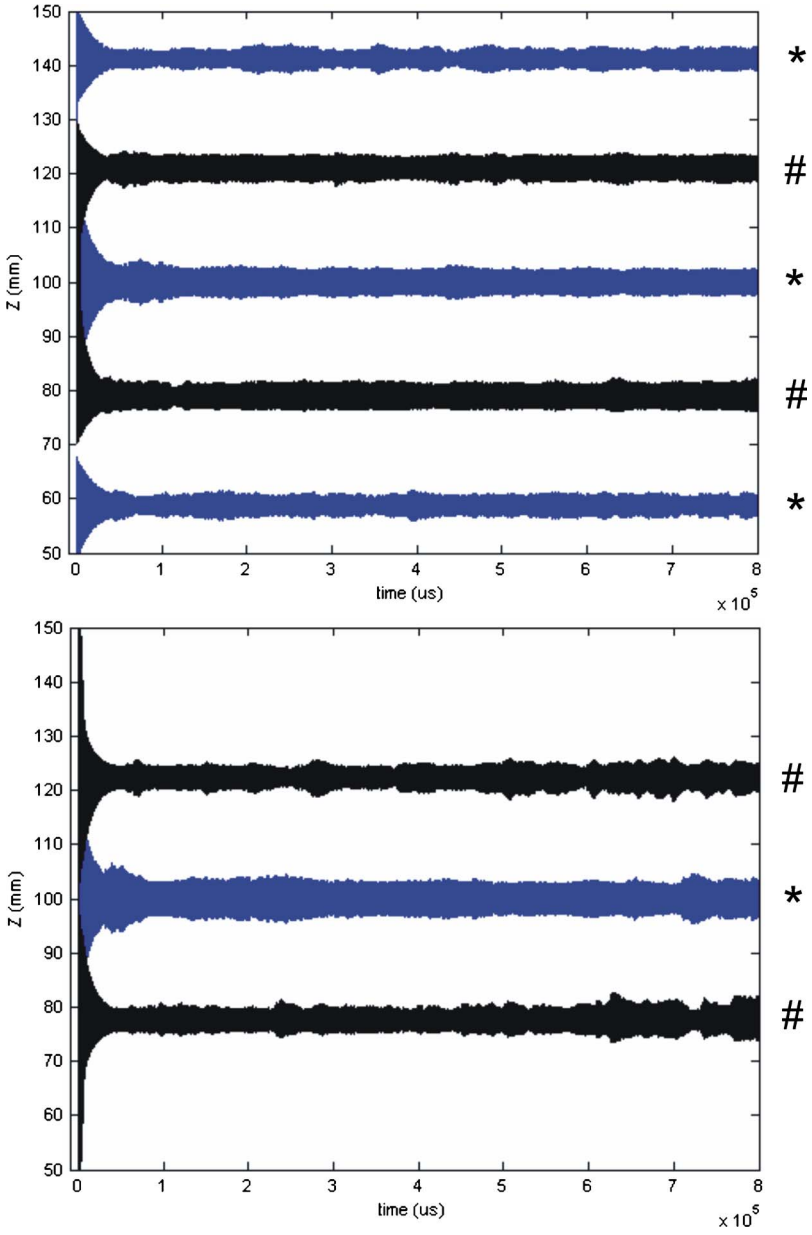

FIG. 3. SIMION simulation of 25 positive ion clouds (SF_5^+) and 25 negative ion clouds (SF_6^-) in (A) the double well potential configuration 0/6/0/6/0 (upper diagram) and (B) the double well potential configuration 1/6/0/6/1 (lower diagram) Positive ions (*); negative ions (#).

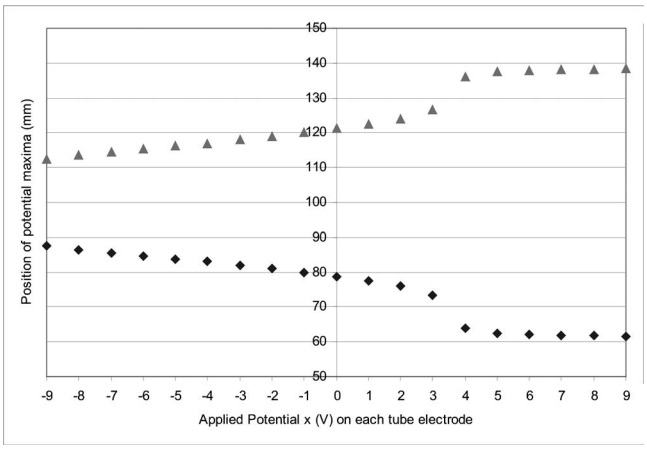

FIG. 4. Position of both potential maxima in the double hill potential configuration $x/6/0/6/x$ as a function of the potential of each tube electrode x(V). At $z=100$ mm (cell center), there is a potential minimum. The whole length of the ICR cell is shown from 50 to 150 mm on the y axis. Detection region is located in axial range (70–130 mm).

ter electrode in regions B and D (cf. Fig. 1). This is the case for both potential configurations 1/6/0/6/1 and 0/6/0/6/0, although the asymmetry of these terminal stability regions is higher in 0/6/0/6/0. Furthermore, deep potential values in the terminal regions B (50–70 mm) and D (130–150 mm) relative to the central potential minimum in the case of 0/6/0/6/0 produce an inward directed axial force, which acts for terminal ion axial stabilization in addition to the fact that this force counters the outward directed axial component of the radial excitation electric field, which affects terminal trapped ions.

Figure 3(a) shows calculated ion trajectories for SF_5^+ and SF_6^- ions in the potential configuration 0/6/0/6/0. Ion trajectories for the same ion types were calculated for 1/6/0/6/1 in Fig. 3(b). In both SIMION simulations, positive ions are initiated along the whole cell length. 25 positive and 25 negative ions were simulated in each run under simulated damping collision and a total Coulumbic interaction of 4×10^{-16} C. Thus nearly 2000 ions from each polarity were simulated simultaneously.

However, ion trajectories in both double well potential configurations 0/6/0/6/0 and 1/6/0/6/1 signalize the distinguished feature of this new design to provide three ion stability regions inside (not outside and near) the detection region BCD (70–130 mm) when this design is compared with a five section open cylindrical ICR cell with two correction electrodes near the central detection region. Figure 4 shows the position of both potential maxima in the potential configuration $x/6/0/6/x$ as a function of the potential x of each tube electrode.

Three stability regions (one central positive and two terminal negative) are sustained within this design even at higher potential values of the tube electrodes till +3 V, when both side electrodes are kept at +6 V relative to the grounded central segmented ring electrode. Figure 4 also shows a nonlinearity of the positions of potential maxima as a function of the applied voltage on each tube electrode in $x/6/0/6/x$. Beyond +3 V of tube electrode potential, the stability regions of the terminal negative ions shift out of the detection

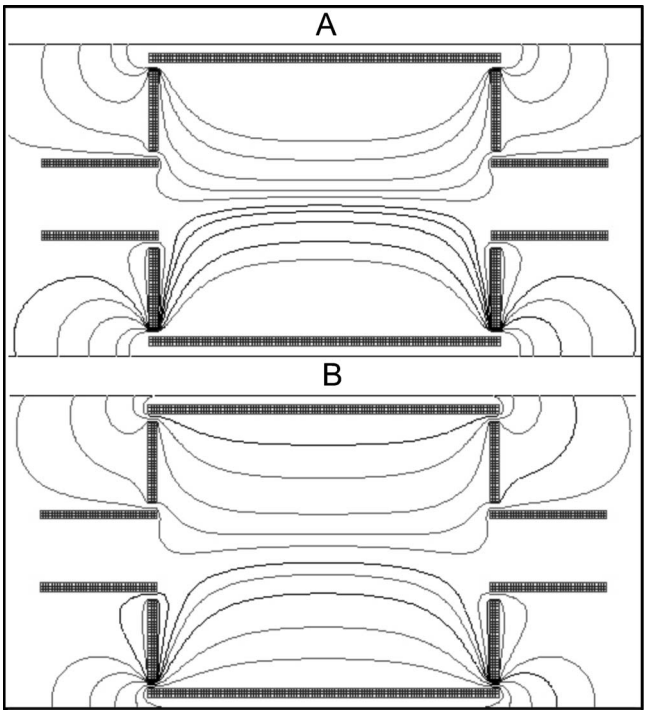

FIG. 5. Equipotential lines for radial excitation electric field (A) at 0 dB (150.8 V p.-p.) and (B) at 5 dB (77.4 V p.-p.) at the axial potential configuration 1/6/0/6/1. Contours shown are (from bottom to top) as follows: −30, −20, −10, −5, −2, +2, +5, +10, +20, and +30 V in each field.

region (70–130 mm), rendering negative ion detection to be difficult in this case. However, deep potential well in the cell center can be created with higher potential of both tube electrodes.

2. Radial excitation patterns within the potential configuration 1/6/0/6/1

The curvature of equipotential lines in the terminal regions within detection area is illustrated in Fig. 5, when a dipolar radial excitation electric field is triggered prior to ion detection. Figure 5(a) shows a curved equipotential line, which is extended more outwards in the stronger radial electric field (0 dB) relative to the field (5 dB) shown in Fig. 5(b). From the curvature and the density of equipotential lines, it is also easy to conclude that the intensity of ion outward acceleration is higher in case (A) and that acceleration vector has more axial component in case (A) relative to case (B).

However, central positive ions should not be affected in both cases, since the axial component of the radial excitation electric field is negligible in the cell center. However, no resolution higher than 1×10^6 could be reached in this geometry even at relatively low pressures of 1×10^{-9} mbar.

SIMION simulations were done to track the final cyclotron radii of central SF_3^+ and terminal SF_6^- trapped within 1/6/0/6/1 in the cell and the central SF_6^- and terminal SF_3^+ ions trapped in the potential configuration −1/−6/0/−6/−1 for comparison. Within this simulation, 15 ms time was set up to allow for ion collisional cooling at damping constant of 1×10^{-4}, before a dipolar radial excitation pulse was triggered from the transmitter segments of the ring electrodes in

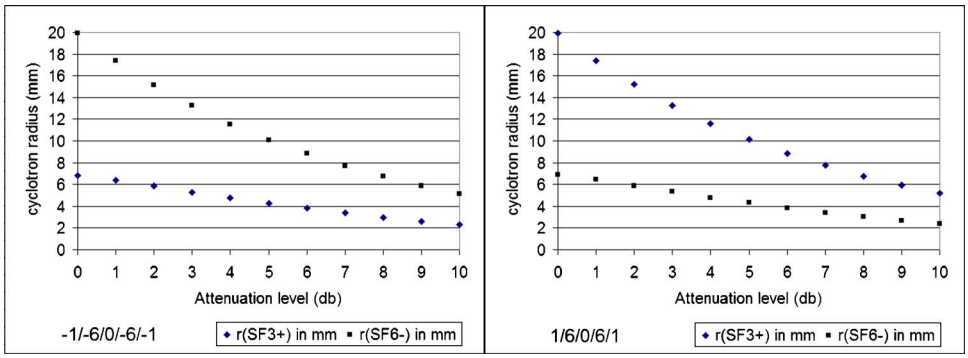

FIG. 6. Cyclotron radii of SF_3^+ and SF_6^- ions vs attenuation level (in decibel) of a radial dipolar excitation electric field for potential configurations $-1/-6/0/-6/-1$ (left) and $1/6/0/6/1$ (right). Within this simulation, final cyclotron radii were registered directly after the end of the radial excitation pulse without any additional delay time to allow for collisional relaxation.

resonance with the cyclotron frequency of SF_3^+ and SF_6^- (signal of two combined sine waves).

Cyclotron radii were calculated directly after the end of the radial dipolar excitation pulse before ion relaxation occurred. Dipolar radial excitation was used and the excitation pulse duration was 100 μs. Figure 6 shows a clear discrimination in radial excitation between central positive and terminal negative ions in $1/6/0/6/1$ and the corresponding clear radial discrimination between central negative ions and terminal positive ions in $-1/-6/0/-6/-1$. Central positive ions can be detected by a factor of 2.5 more efficiently than terminal negative ions when an attenuation level of 2 dB (115.5 V p.-p.) is used in the potential configuration $1/6/0/6/1$. Such a ratio could be obtained experimentally too at 2×10^{-7} mbar. The same is true for central negative ions relative to the terminally trapped positive ions within the simulation in the configuration $-1/-6/0/-6/-1$.

In an effort to explain the large discrimination of detection between positive and negative ions shown previously in case of $1/6/0/6/1$, we have decided to look at axial potential course in $1/6/0/6/1$ at different cyclotron radii. These potential patterns are shown in Fig. 7.

In the cyclotron radius range from 0 to 7 mm, there is a double hill potential configuration. However, the terminal potential hills shift axially outwards when the excited ions gain greater cyclotron radii through radial acceleration.

As the cyclotron radius of ions increases greater than 7 mm, there is a radical change in the form of effective potential configuration along the z axis. For cyclotron radii above 7 mm, the effect of the interfering electric field of the side electrodes S1 and S2 is obvious. The effective potential form changes from double hill to one potential well suitable for trapping positive ions only. Thus, as negative ions reach cyclotron radius of 8 mm, they can be ejected axially outwards, since their terminal stability regions (indicated by the two terminal potential hills) shift more outwards till $r=7$ mm. Above this cyclotron radius, no negative ions can still be trapped axially, since no double hill potential configuration exists.

As indicated above from Fig. 2, the stability regions of terminal negative ions in the potential configuration $1/6/0/6/1$ are located at z values of 77.5 and 122.5 mm. Let us see what form of radial electric potential distribution is available at the terminal stability region of negative ion indicated by $z=77.5$ mm and the central stability region of positive ions indicated by $z=100$ mm.

As illustrated in Fig. 8(b), the radial potential curve in the central region ($z=100$ mm) of $1/6/0/6/1$ is normal for classical ICR cells. However, the double hill radial potential curve [Fig. 8(a)] in the terminal stability regions, which is responsible for trapping negative ions in $1/6/0/6/1$ terminally, is unusual and sharply asymmetric. In addition, the latter has high effective potential values. The same difference in the radial potential distribution pattern between central and terminal regions in the potential configuration $-1/-6/0/-6/-1$ exists [see curves (C) and (D) in Fig. 8].

If we return back to the radial potential pattern of the terminal negative stability regions in the potential configuration $1/6/0/6/1$ [Fig. 8(a)], we notice that the potential maxima at $y=51.5$ mm and $y=28.5$ mm represent cyclotron

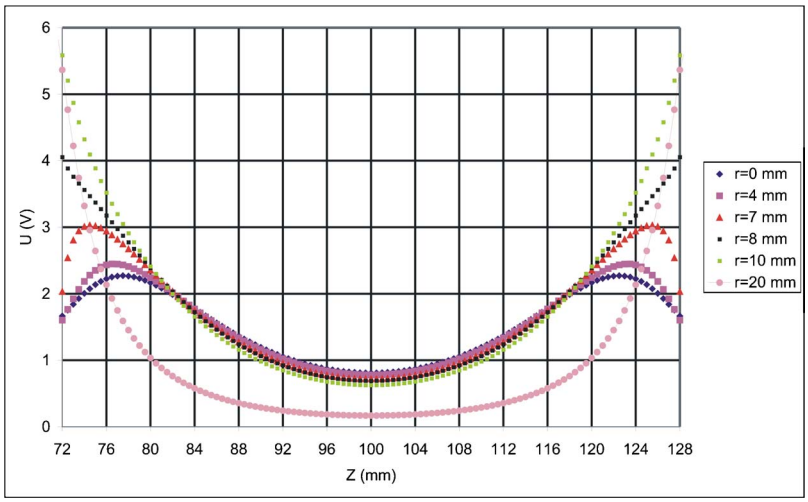

FIG. 7. Axial potential course in several radial planes, defined by variable radius in millimeter. Applied potential configuration is $1/6/0/6/1$.

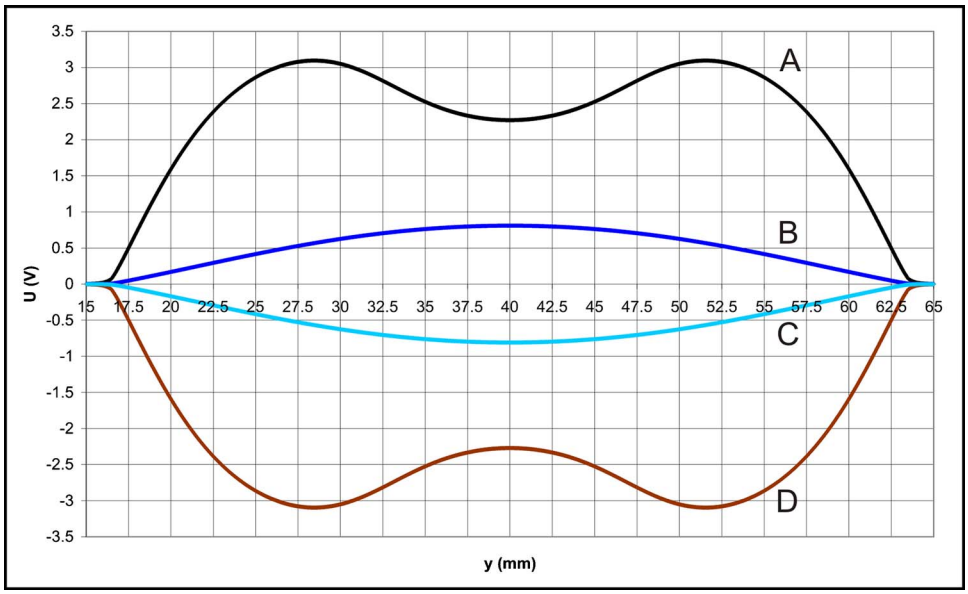

FIG. 8. Radial effective electric potential curves at (A) terminal stability region $z=77.5$ mm (double hill potential configuration shown in black, terminal negative ions) in the potential configuration 1/6/0/6/1, (B) central stability region (one potential hill shown in dark blue, positive ions) at $z=100$ mm in 1/6/0/6/1, (C) central stability region (one potential well shown in light blue, negative ions) at $z=100$ mm in −1/−6/0/−6/−1, and (D) terminal stability region $z=77.5$ mm (double well potential configuration shown in brown, terminal positive ions) in the potential configuration −1/6/0/−6/−1.

radius of 11.5 mm, which appears to be the maximum cyclotron radius reached by radially excited terminal negative ions. However, Fig. 6 shows a maximum radius of just 7 mm, which can be reached by terminal negative ions, if they are radially excited by a dipolar radial excitation electric field with attenuation level of 0 dB.

The difference between these mentioned postexcitation cyclotron radii of negative ions ($r=11.5$ and $r=7$ mm) in 1/6/0/6/1 can be justified by the sharp radial asymmetry of the double hill effective potential curve shown in Fig. 8(a). The cyclotron radius of postexcited terminal negative ions cannot really exceed 7 mm, since a radially inward directed electric force acts above $r=7$ mm to hinder further increase of the cyclotron radius of negative ion during radial dipolar excitation in 1/6/0/6/1. The axial component of the excitation radial electric field is another factor, which limits the increase of cyclotron radius of terminal ions during radial excitation event in 1/6/0/6/1.

As a result of the large difference between the radial electric potential pattern in the central stability region, where positive ions in 1/6/0/6/1 can be trapped, and the radial potential pattern in the terminal stability regions for negative ions, ions can be accelerated differently in radial direction by the dipolar radial excitation electric field. Figure 9 illustrates the three-dimensional (3D) electric potential distribution inside the detection region of the new ICR cell within 1/6/0/6/1 and −1/−6/0/−6/−1 potential configurations.

The difference in radial acceleration magnitude of positive and negative ions trapped in different stability regions has a strong effect on the postexcitation total kinetic energy gain. On the other hand, radial energy dissipation is dominant in both ion polarities, since an axial acceleration component exists during radial excitation event. However, axial acceleration component is greater in the case of terminally trapped ions and this also contributes to the limitation ap-

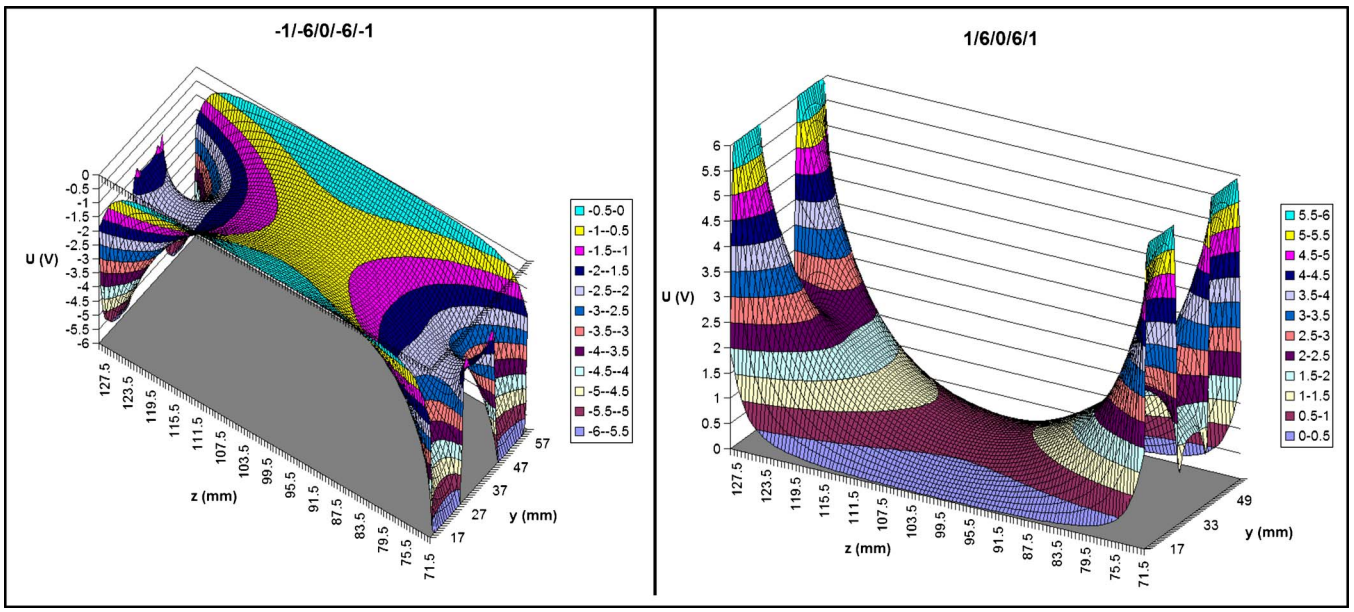

FIG. 9. 3D view of the electric potential distribution in the yz plane in the potential configurations −1/−6/0/−6/−1 (left) and 1/6/0/6/1 (right).

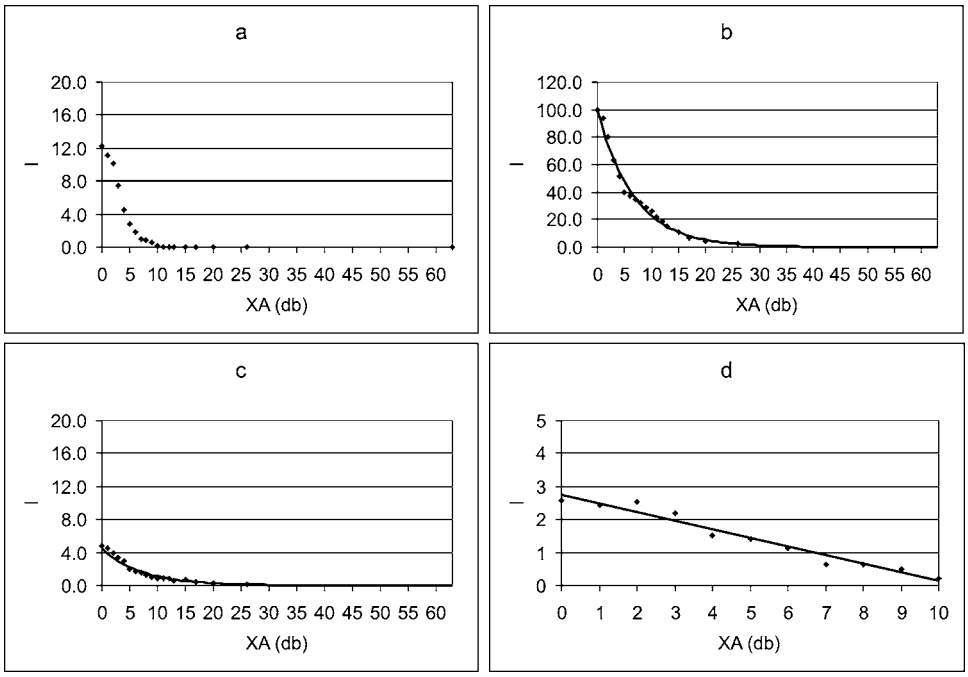

FIG. 10. Ion signal intensity change as a function of attenuation level XA (in decibel) of the excitation radial electric field at 2×10^{-7} mbar. (a) SF_3^+, (b) SF_5^+, (c) SF_6^+, (d) and SF_3^+/SF_6^- present.

plied on the increase of the cyclotron radius of terminally trapped ions during radial excitation in comparison with that of central ions, regardless whether 1/6/0/6/1 or −1/−6/0/−6/−1 configuration is used.

C. Experimental results

1. Positive and negative ion detection as a function of radial dipolar excitation field strength in 1/6/0/6/1

Figure 10 shows the dependence of signal intensity on the attenuation level of the radial dipolar excitation electric field used prior to simultaneous positive and negative ion detection within 1/6/0/6/1. All curves show exponential behavior, which corresponds to the linearity of ion detection. Even when the cell is saturated with SF_5^+ ions trapped in the central region, SF_3^+/SF_6^- ratio is not constant and it is higher than 1 at higher excitation field strength (attenuation levels lower than 6 dB). The SF_3^+/SF_6^- ratio becomes higher than 2.5 at attenuation levels lower than 3 dB and this stands in correlation with the SIMION simulations shown previously for post-radial-excitation of the cyclotron motion of both ion polarities in 1/6/0/6/1.

2. Trapping effectivity of the cell in 1/6/0/6/1 and −3/3/0/3/−3 at 2×10^{-6} mbar

Figure 11 shows the result of a trapping efficiency test done for SF_3^+ and SF_6^- in the potential configuration 1/6/0/6/1 [parts (a) and (b)] and in the potential configura-

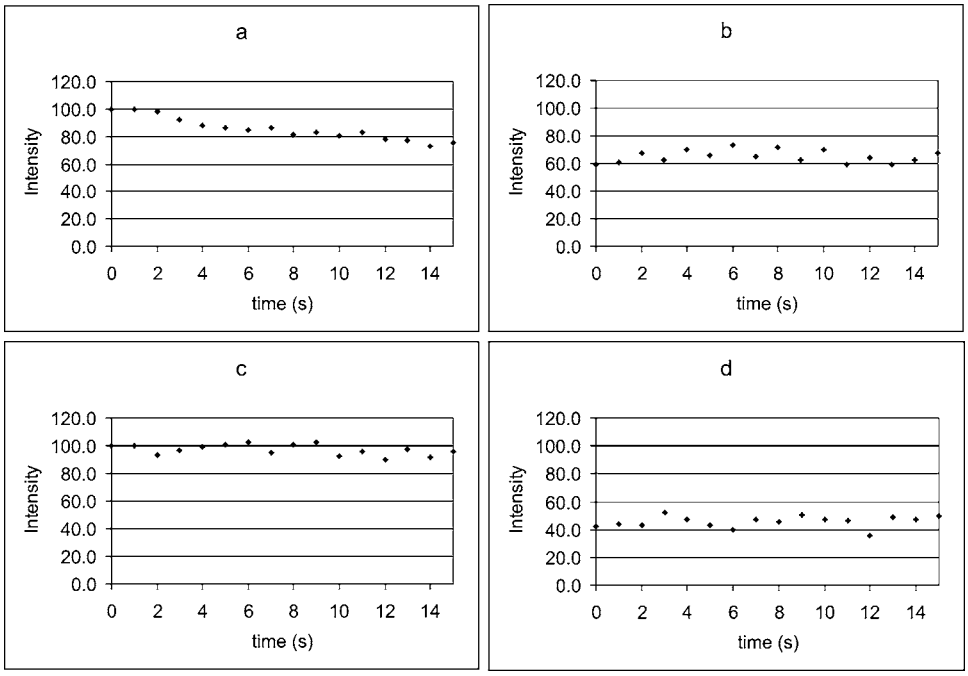

FIG. 11. Dependence of ion signal intensity on the trapping time at 2×10^{-6} mbar for (a) SF_6^- in 1/6/0/6/1, (b) SF_3^+ in 1/6/0/6/1, (c) SF_6^- in −3/3/0/3/−3, and (d) SF_3^+ in −3/3/0/3/−3.

tion −3/3/0/3/−3 [parts (c) and (d)] at relatively high pressure of 2×10^{-6} mbar. Both positive and negative ions can be trapped efficiently in the potential configuration −3/3/0/3/−3 under high pressure (2×10^{-6} mbar).

While positive ions in 1/6/0/6/1 trapped in the central region of the cell can be retained for 15 s at 2×10^{-6} mbar, terminal SF_6^- ions show partial loss as a function of the trapping time in case of 1/6/0/6/1. This partial loss is due to the outward directed radial electric force applied on the terminal stability regions shown in Fig. 8. Thus, terminal negative ions do not remain radially confined in the radial plane *xy*. They draw a magnetron evolution as a function of time.

Both positive and negative ions can be trapped and detected simultaneously in a static double hill potential configuration in this new ICR cell. The double hill potential configuration 1/6/0/6/1 was studied intensively. Comparison between the potential configurations 1/6/0/6/1 and −1/−6/0/−6/−1 was made. Axial potential distributions reveal asymmetric terminal stability regions relative to a symmetrical central region. The axial component of the radial excitation electric field exists in the terminal stability regions and plays a role in dissipating kinetic energy during radial excitation. A sharp discrimination in radial dipolar excitation between positive and negative ions was shown both experimentally and theoretically. In depth analysis of electric potential distribution patterns provide explanations to the observations. Within the potential configuration 1/6/0/6/1, positive ions can be trapped more efficiently than negative ions at extremely high pressure of 2×10^{-6} mbar, while both ion polarities can be trapped with high efficiency in −3/3/0/3/−3 at high pressure. Due to the radial discrimination between different ion polarities in 1/6/0/6/1 shown above, specific collisional fragmentation could be induced only for central positive ions, even if negative ions with same m/z ratio are trapped simultaneously in the terminal regions of this ICR cell.

ACKNOWLEDGMENTS

One of the authors (B.K.) would like to thank the Verband der Chemischen Industrie (VCI) for a Ph.D. grant. The authors also thank W. Fulda and his co-workers in the mechanical shop for building the new ICR and for providing continuous mechanical support.

[1] A. G. Marshall, C. L. Hendrikson, and G. S. Jackson, Mass Spectrom. Rev. **17**, 1 (1998).
[2] S. E. Barlow and M. D. Tinkle, Rev. Sci. Instrum. **73**, 4185 (2002).
[3] G. Gabrielse, L. Haarsma, and S. L. Rolston, Int. J. Mass. Spectrom. **88**, 319 (1989).
[4] W. W. Yin, M. Wang, A. G. Marshall, and E. B. Ledford, J. Am. Soc. Mass Spectrom. **3**, 188 (1992).
[5] S. Guan and A. G. Marshall, Int. J. Mass. Spectrom. **146/147**, 261 (1995).
[6] G. Bollen *et al.*, Nucl. Instrum. Methods Phys. Res. A **368**, 675 (1996).
[7] D. Beck *et al.*, Eur. Phys. J. A **8**, 307 (2000).
[8] G. Gabrielse and F. C. Mackintosh, Int. J. Mass. Spectrom. **57**, 1 (1984).
[9] G. Gabrielse, S. L. Rolston, and L. Haarsma, Phys. Lett. A **129**, 38 (1988).
[10] R. A. Zubarev, N. L. Kelleher, and F. W. McLafferty, J. Am. Chem. Soc. **120**, 3265 (1998).
[11] J. E. P. Syka, J. J. Coon, M. J. Schroeder, J. Shabanowitz, D. F. Hunt, and F. W. McLafferty, Proc. Natl. Acad. Sci. U.S.A. **101**, 9528 (2004).
[12] E. R. Badman, P. A. Chrisman, and S. A. McLuckey, Anal. Chem. **74**, 6237 (2002).
[13] Y. Wang and K. P. Wanczek, Rev. Sci. Instrum. **64**, 883 (1993).
[14] V. H. Vartanian and D. A. Laude, Org. Mass Spectrom. **29**, 692 (1994).
[15] R. Malek and K. P. Wanczek, Rapid Commun. Mass Spectrom. **11**, 1616 (1998).
[16] D. A. Dahl, SIMION 7, Idaho National Engineering and Environmental Laboratory, Idaho Falls, ID.
[17] J. J. Drader, S. D.-H. Shi, G. T. Blakney, C. L. Hendrickson, D. A. Laude, and A. G. Marshall, Anal. Chem. **71**, 4758 (1999).